Promoter-poison partnership protects platinum performance in coked cluster catalysts

Patricia Poths,*,† Harry W. T. Morgan,† Guangjing Li,‡ Autumn Fuchs,‡ Scott L. Anderson,*,‡ and Anastassia N. Alexandrova*,†,¶

†*Department of Chemistry and Biochemistry, University of California, Los Angeles, Los Angeles, CA 90095, USA*

‡*Department of Chemistry, University of Utah, Salt Lake City, UT, 84112, USA*

¶*California NanoSystems Institute, Los Angeles, CA, 90095, USA*

E-mail: patriciapoths@chem.ucla.edu; anderson@utah.edu; ana@chem.ucla.edu

Abstract

Deactivation via coking due to a lack of selectivity is a persistent problem for the longevity of Pt-based dehydrogenation catalysts. Ge as a promoter improves the experimental selectivity and stability of subnano Pt clusters. The origin of this improvement is self-limiting coking, to form a Pt_4GeC_2 cluster which is more stable and selective than the bare Pt_4Ge cluster. In this paper we compare the dehydrogenation abilities of Pt_4 and Pt_4C_2 with and Pt_4Ge and Pt_4GeC_2 with DFT calculations in order to explore the origin of self-limiting coking in the presence of Ge. The unique stability of Pt_4GeC_2 is attributed to electron donation from Ge to the C_2 atoms. This prevents the coke from drawing electrons from the Pt, which is the origin of deactivation via coking. Thus, we identify an electronic mechanism for coke deactivation and then use an electronically driven doping strategy to improve catalyst longevity. This differs from the common perception of coke deactivating via steric blocking of active sites.

Furthermore, Pt_4C_2 and Pt_4GeC_2 show differences in kinetic accessibility of different isomers, which brings us into a new paradigm of sub-ensembles of isomers, where the dominant active sites are determined by kinetic stability under reaction conditions, rather than Boltzmann populations.

Introduction

The formation of coke, or carbonaceous deposits, is a persistent problem for dehydrogenation catalysts, as it results in their rapid deactivation. Deactivation is typically attributed to physical blocking of active sites on the catalyst. Coke formation on Pt-based alkane dehydrogenation catalysts originates from the lack of selectivity of the catalyst; side reactions for deeper dehydrogenation past alkenes and C-C cracking contribute to coke formation. Approaches to preventing coke formation include co-feeding H_2,[1] changing Pt nanoparticle size,[2] and dopants or promoters such as Sn,[3–5] Ge,[6,7] Si,[8] Ga,[9–11] Zn,[12] and B.[13–15] These approaches all favor desorption of the desired alkenes over deeper dehydrogenation (or cracking) reactions.

Coke formation typically occurs in two stages; an initial fast coking regime, and a later regime where the buildup of further coke is much slower,[16,17] which indicates that early coking stages change catalysts selectivity to limit further coking. This change in selectivity has been attributed to carbon blocking the most reactive and least selective sites, which can catalyze side-reactions leading to coke formation.[18–23] An additional explanation is that the presence of carbon can modify olefin adsorption strength on a surface, and increase the energy barrier for C-H activation.[17] Coke may therefore deactivate Pt catalysts via an electronic interaction, in addition to steric blocking.

The interaction between metal and coke influencing selectivity is reminiscent of dopants or promoters; the selectivity improvement from adding Sn or Ge to the Pt catalyst comes at the cost of activity, though not to the same extent as coking. Sn is the most widely-used dopant for Pt, though Ge has been found to produce similar improvements in stability against cok-

ing.[20–23] XPS of subnano PtSn clusters shows a shift to lower binding energies, implying that Sn tends to donate electrons to Pt.[3] However, there have been reports that PtSn catalysts build up more coke than their pure Pt analogues,[24] suggesting that they are not simply resistant to the build-up of coke, but that their activity persists despite partial coking. The contrast between the electronic and steric mechanisms of coking, and the role of doping are represented in Figure 1.

Sub-nano clusters are promising catalysts due to their high atom utility, and ability to

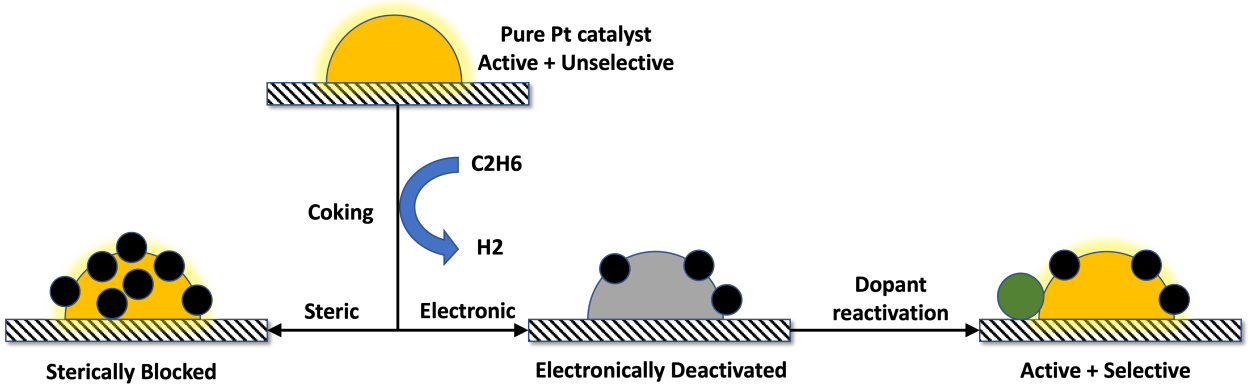

Figure 1: Schematic showing the steric and electronic deactivation mechanisms of coked platinum catalysts, and the activity-restoring effect of doping on electronically deactivated catalysts.

outperform bulk-like catalysts by breaking scaling relations.[25] Pure Pt clusters have been studied as alkane dehydrogenation catalysts,[26] as have various dopants to improve catalyst selectivity, including B,[14] Si,[8] Ge[7] Sn,[3–5] and S.[27] Surface-supported clusters are fluxional, isomerizing rapidly under the high temperatures of real reactions such that metastable structures are thermally populated.[28] Higher-energy isomers often show greater catalytic activity than the global minimum isomer.[29–31] If the kinetic barriers for isomerisation are low, then the isomer populations will be determined by a Boltzmann distribution.[32] If a cluster were to have high isomerisation barriers then the ensemble would not thermally equilibrate, and macroscopic properties would be determined by the reduced set of accessible isomers, which could be useful if the prevalent isomers have superior activity.[33]

Our most recent work focused on Al_2O_3-supported PtGe subnanoclusters, which were pre-

pared experimentally after Ge was theoretically predicted to be a suitable dopant.[7] We found that not only were the prepared Pt_4Ge clusters reasonably stable and selective, but that they slowly converted to a partially-coked form, Pt_4GeC_2, which was stable against further coking.[29] This parallels the behavior of PtSn nanoparticles which remain active and stable despite building up more coke than their pure Pt analogues.[24] Transforming a poisoning process into in-situ catalyst synthesis by doping, illustrated in the right-most part of Figure 1 is a powerful new strategy in catalyst design. To apply this strategy to other reactions, we must first understand the fundamental chemistry behind the efficacy of Pt_4GeC_2. In this paper we investigate the electronic synergy between Ge and coke in Pt_4 clusters in the context of ethane dehydrogenation with a combination of DFT calculations and experiment. For the DFT calculations, we focus on the "pristine" clusters Pt_4 and Pt_4Ge, and their partially coked counterparts Pt_4C_2, and Pt_4GeC_2. After obtaining the ensemble of isomers, we perform transition state calculations to obtain barriers and determine the reactivities of these isomers towards ethane and ethylene dehydrogenation. Detailed bonding analyses of the interaction between Ge and C_2 provides deeper chemical insights into activity and stability trends. With supporting experimental evidence from ISS and TPD data, we observe that Ge mitigates the deactivating effect of C towards ethane dehydrogenation, and improves the selectivity towards ethylene desorption.

Results and discussion

Pt_4 and Pt_4C_2

Pt, in the bulk or in the nanoparticle/cluster form, is a facile catalyst for ethane dehydrogenation, and Pt_4 is no exception to this, proving to bind ethane and activate C-H bonds with low activation barriers based on DFT calculations (vide supra). However, Pt suffers from lack of selectivity, and it has been shown both experimentally and computationally to dehydrogenate ethylene and acetylene, leading to rapid deactivation by coking. "Complete

dehydrogenation" of ethane adsorbed on Pt_4 forms a Pt_4C_2 cluster, which may be seen as the first step of coking. To assess theoretically the effects of this initial coking on catalytic activity and selectivity in subsequent reactions we must first explore the isomeric ensembles of Pt_4 and Pt_4C_2. Here we explore the initial coking product Pt_4C_2 and directly compare it to Pt_4GeC_2, which is found to be selective and stable against further coking.[29] Furthermore, this gives us useful information about early stages of coking. Relevant isomers for Pt_4C_2/Al_2O_3 obtained via global optimization can be seen in Figure 2(a); see Figure S1 for the Pt_4/Al_2O_3 and $Pt_4C_{2/}Al_2O_3$ full ensembles. The C atoms are mostly 3-coordinate while the Pt atoms are on the edges of the clusters, so incorporation of C into the Pt_4 cluster does not block Pt sites. Incorporation of C into the Pt cluster results in dramatic structural differences between the Pt_4 and Pt_4C_2 ensembles. Clearly, the earliest stages of coke formation induce structural reorganization.

To compare the reactivity and selectivity of Pt_4/Al_2O_3 and Pt_4C_2/Al_2O_3, we computed the binding modes of ethane, ethylene, and acetylene to the thermally accessible isomers of both clusters. The accessible binding modes can be seen in Figure S2. We then computed the first C-H activation barriers for low-energy binding modes as a descriptor for the activity or selectivity of Pt_4/Al_2O_3 and Pt_4C_2/Al_2O_3.

Reactivity studies of fluxional systems are challenging because we must understand the contribution of each isomer to the overall reactivity. Using the Curtin-Hammet principle, where the distribution of products is determined by the free energy difference between the two transition states, $\Delta\Delta G^{\ddagger}$, we consider the isomer with the lowest transition state energy relative to the global minimum the driver of reactivity for that step.[33,34] To show this for our multi-component systems, we plot barriers on bar charts where all energies are given relative to the global minimum for that composition in Figure 2(b,c). Therefore, accoridng to the Curtin-Hammet principle, the most reactive isomers are the ones with the lowest bar tops in Figure 2(b,c).

C-H activation barriers for Pt_4 and Pt_4C_2 are shown for ethane in Figure 2(b) and for ethy-

lene in Figure 2(c). Results for acetylene can be found in Figure S3 along with details of all computed barriers (Figure S4). Figure 2(b) shows that Pt_4 is an active dehydrogenation

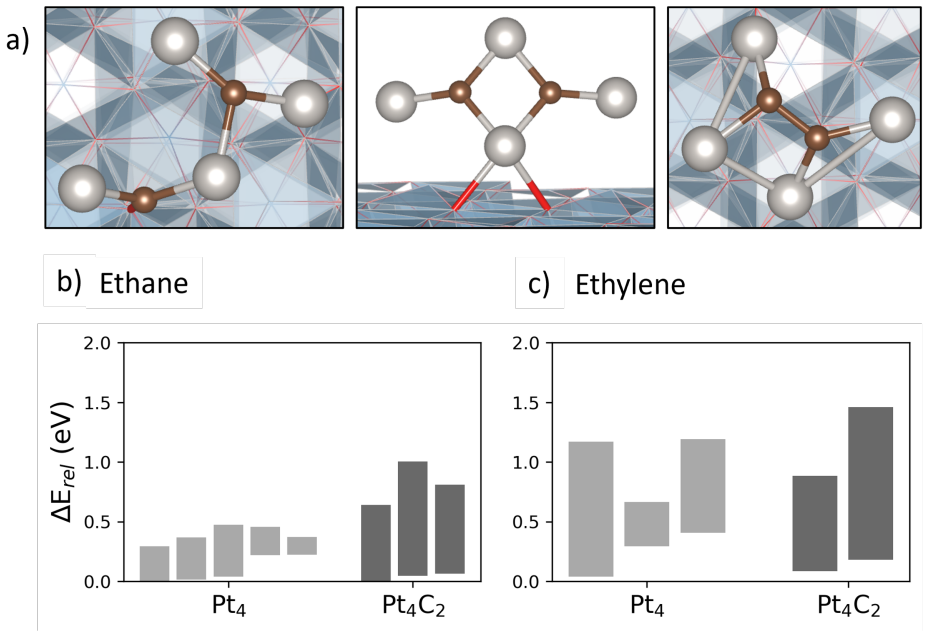

Figure 2: (a) Low-energy isomers of Pt_4C_2. Pt atoms are shown in grey, and C atoms in brown. Blue polyhedra represent the Al_2O_3 support. (b,c) Ethane and ethylene (respectively) C-H activation barriers for Pt_4 and Pt_4C_2 with individual isomer resolution. The bottom of each bar corresponds to the energy of the reactant isomer, relative to the lowest energy isomer for that composition, and the top of each bar corresponds to the transition state energy.

catalyst for ethane, with computed transition state energies as low as 0.29 eV above the ground state. When C_2 is added to the Pt_4 cluster, the barriers for ethane C-H activation increase to 0.64 eV, showing that a small amount of coke has a large deactivating effect. We also see an increase in the lowest ethylene C-H activation barrier for Pt_4C_2 relative to Pt_4, indicating an increase in selectivity (Fig. 2(c)). This agrees with literature;[17] even the inclusion of a small amount of carbon on Pt, either in bulk, or larger more bulk-like NPs will dramatically reduce the activity towards ethane dehydrogenation, while improving selectivity towards ethylene. The charge distributions in Figure 3(a,b), calculated using QTAIM,[35] reveal details of the mechanism of electronic deactivation. The carbon atoms are negatively charged, having drawn electron density away from the platinum atoms, as expected from

Pauling electronegativity values.[36] A similar charge-transfer effect has been observed experimentally in S-doped Pt catalysts by XPS and CO stretching frequencies.[27] With this in mind, we next investigate the efect of Ge doping on catalyst stability and selectivity.

Pt_4Ge and Pt_4GeC_2

Pt_4Ge is a stable and selective candidate catalyst for ethane dehydrogenation,[29] and both experiment and theory suggest that the partially coked species Pt_4GeC_2 is actually the stable form of the catalyst. The low-lying isomers of Pt_4GeC_2 fall into two groups - those with separated C atoms, and those with a C−C dimer, both of which are shown in Figure 4(a) (see figure S5 for the full Pt_4Ge and Pt_4GeC_2 ensembles). Note the similarities in the Pt-C binding between Pt_4C_2 (Figure 2a) and Pt_4GeC_2 (Figure 4a); the inclusion of C_2 induces similar restructuring with and without Ge. This means that Ge in Pt_4GeC_2 is not altering the reactivity due to a stabilization of Pt core structures different from those of Pt_4C_2. As a result, the stabilization of Pt_4GeC_2 against further coking and deactivation must have an electronic cause.

Consider the lowest-energy isomer of Pt_4GeC_2 with a bonded C−C dimer (Figure 4(a), right side), which lies just 0.06 eV above the global minimum isomer (which has separated C atoms, Figure 4(a), left side), and compare it to the corresponding isomer of Pt_4C_2. There are several reasons for focusing on these C-C bonded isomers. The isomer populations would be thermally equilibrated, and thus dominated by the global minimum structures if the barriers to isomerisation were low (e.g. in undoped Pt_7),[28] but in this case, the computed barrier is ˜ 1.33 eV, indicating that interconversion should be slow. Furthermore, based on the active structures for ethylene dehydrogenation, we expect that the C-C bonded isomer should dominate Pt_4GeC_2 formation, and remain dominant because of the high isomerization barrier. This is important because the global minimum isomer of Pt_4GeC_2, with separated C atoms, is predicted to be unreactive towards ethane, based on its lack of chemisorption of ethane in DFT calculations (Figure S6), whereas the C-C bonded isomer should be reactive,

based on our activation energy calculations.

Figure 3(a,b) shows these active isomers of Pt_4C_2 and Pt_4GeC_2 annotated with atomic QTAIM charges. The large positive charge on Ge indicates electron-donating behaviour, while the negative charges on C show electron acceptance, in agreement with electronegativities. The Pt atomic charges vary, but the sums (-0.10 for Pt_4C_2, -0.50 for Pt_4GeC_2) indicate that electron donation from Ge to Pt compensates for the electron depletion by transfer to carbon.

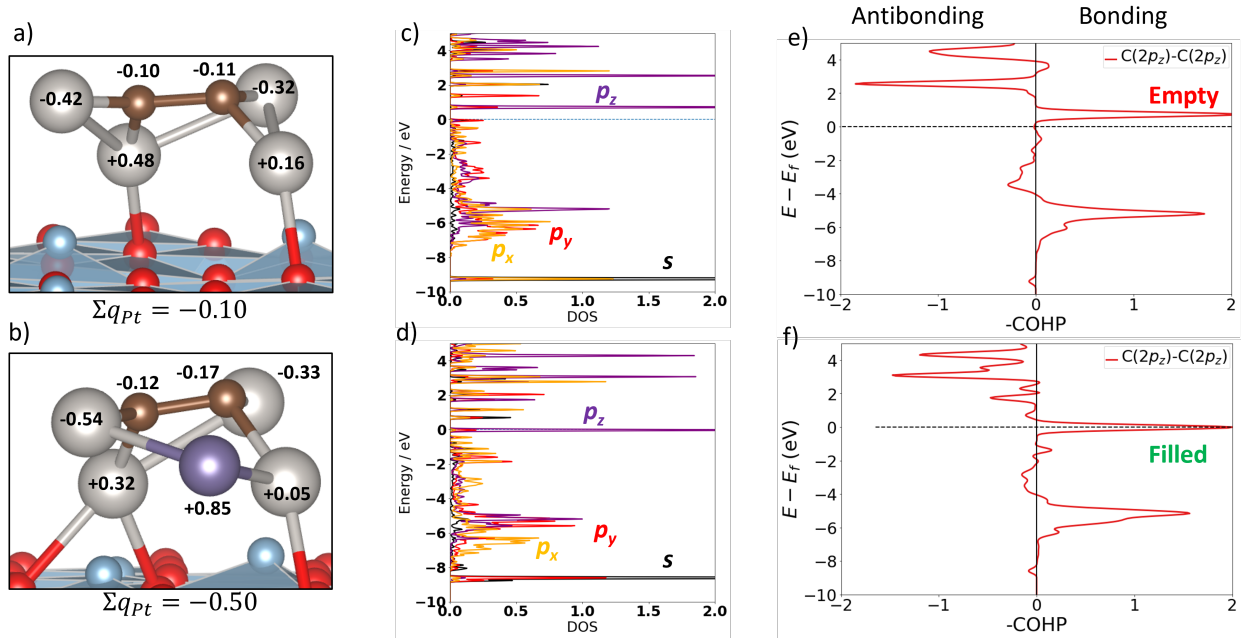

Figure 3: Electronic structure and bonding properties of active isomers of $Pt_4(Ge)C_2$. (a,b) Structures of Pt_4C_2 and Pt_4GeC_2 on Al_2O_3 with Pt shown in grey, C in brown, and Ge in purple, Al in blue, and O in red. Each atom is labelled with its computed QTAIM charge, and Σq_{Pt} denotes the sum of the Pt charges. (c,d) Projected density of states (PDOS) plots for the $2s, p$ orbitals of carbon annotated with p_z Mulliken populations. The $2s$ PDOS is in black, p_x in orange, p_y in red, and p_z in purple. (e,f) ICOHP plots for the C $2p_z$- C $2p_z$ interaction, annotated with the C-C atomic ICOBI.

To further study the bonding in Pt_4GeC_2 and Pt_4C_2, we devised simple gas-phase models by taking the cluster structures from periodic optimization and deleting the support entirely. The models are validated by their QTAIM charge distributions, which show the same trends as the supported clusters. The molecular clusters, QTAIM charges, and MO diagrams are

shown in Figure S7. The MO diagrams show that the Ge atom in Pt_4GeC_2 is in the +2 oxidation state; the lowest three unoccupied levels have predominant Ge 4p character, while the Ge 4s-based MO is found far below the HOMO. The LUMO of Pt_4C_2, which corresponds to the HOMO in Pt_4GeC_2 after accepting an electron pair from Ge, is C-C π bonding, so adding Ge to Pt_4C_2 strengthens the C-C bonding.

Returning to the supported cluster model, Figure 3(c,d) shows the projected density of states (PDOS) for the carbon 2p orbitals in Pt_4C_2 and Pt_4GeC_2 respectively. The sharp $2p_z$ peak just above E_F in Pt_4C_2 but immediately below E_F in Pt_4GeC_2 suggests a C $2p_z$ orbital that is empty in Pt_4C_2 but filled in Pt_4GeC_2. The C $2p_z$ orbital is perpendicular to the surface, so this PDOS analysis supports the theory that Ge strengthens C-C π bonding. Mulliken analysis also supports this conclusion, showing an increase in C $2p_z$ population from 0.86 to 1.01 on addition of Ge to Pt_4C_2. The most compelling evidence for Ge strengthening C-C bonding is shown in the C $2p_z$ COHP plots in Figure 3(e,f), related to the atomic C-C COHP plots previously reported,[29] and the integrated crystal orbital bond index (ICOBI) values for the C-C atomic pair. COHP shows the bonding character of electronic states between specific pairs of atoms or orbitals, where bonding states appear to the right of the vertical axis (note that the horizontal axis plots -COHP so that positive values denote bonding orbitals). The PDOS peaks around the Fermi level, as discussed above, are present in the bonding channel on the COHP plots, indicating that these states have strong C-C bonding character. ICOBI is a bond order for pairs of atoms in solids,[37] so the increase in C-C ICOBI from 1.20 to 1.55 on addition of Ge is further evidence for a strengthened C-C bond. We can therefore conclude that the Ge dopant donates electrons to C, so Pt remains electron-rich and reactive, while remaining selective.[17,38] The donated electrons occupy a π_{C-C} bonding orbital, so Ge doping strengthens C-C bonding as indicated by the gas phase models.

The isomeric structures for adsorbed hydrocarbons found by global optimization show the consequences of these electronic structure trends. If we compare the first and last isomers of Pt_4C_2 in Figure 2(a) with the isomers of Pt_4GeC_2 in Figure 4(b), we see structural sim-

ilarities, even though these clusters have different reactivities. The binding sites for ethane and ethylene on Pt_4C_2 and Pt_4GeC_2 are similar (Figure S1, S5), consistent with the hypothesis that Ge influences reactivity electronically. There is also a significant Ge effect on the energetics of the isomers with separated vs bonded C atoms. In Pt_4C_2 the C-C bonded isomer lies +0.17 eV above the C-C separated isomer, while in Pt_4GeC_2 the corresponding gap is reduced to +0.06 eV due to C-C bond strengthening by electron transfer from Ge. Furthermore, the equivalent barrier for breaking the C-C bond in Pt_4C_2 (1.16 eV) is lower than that for Pt_4GeC_2 (1.33 eV). See Table S1, and Figure S8 for details.

To quantify the effect of changes in electronic structure on catalytic behavior, 4 shows our previously reported reaction barriers for ethane (Figure 4(b)) and ethylene (Figure 4(c))[29] plotted in the same style as in Figure 2. There is an increase in the ethane C-H activation barrier upon the deposition of C_2, to 0.53 eV but this increase is less than in the absence of Ge, in Figure 2, where the barrier increased to 0.64 eV. Thus, doping with Ge allows the cluster to remain more active for ethane C-H activation after partial coking.

Figure 4(c) shows that the lowest barrier for C-H activation of ethylene increases upon coking, from 1.24 eV in Pt_4Ge to 1.41 eV in Pt_4GeC_2, so the first C_2 deposition should hinder further coking. Doping with Ge increases the ethylene dehydrogenation barriers substantially, from 0.66 eV for Pt_4 to 1.24 eV for Pt_4Ge, so Ge also preserves catalyst activity by reducing the rate of initial coking. Our bonding analysis helps to explain the resistance of Pt_4GeC_2 to further coking. Dehydrogenation of additional ethylene molecules would result in C-C bond formation between the cluster C_2 unit and the subsequently deposited C atoms. Ge strengthens π bonding in the C_2 unit which would have to be broken to bind additional coke, so the combined electronic effects of Ge and C_2 hinder further coking. This manifests in different binding energies of ethylene to Pt_4C_2 (-1.85 eV) and Pt_4GeC_2 (-2.10 eV), for structures where ethylene binds directly to the C_2 unit in the cluster (Figures S4 and S9).

C-C cracking is another side reaction which frequently deactivates pure Pt catalysts.[16,17] In order to assess the role of C-C cracking in coking for Pt_4, Pt_4C_2, Pt_4Ge, and Pt_4GeC_2,

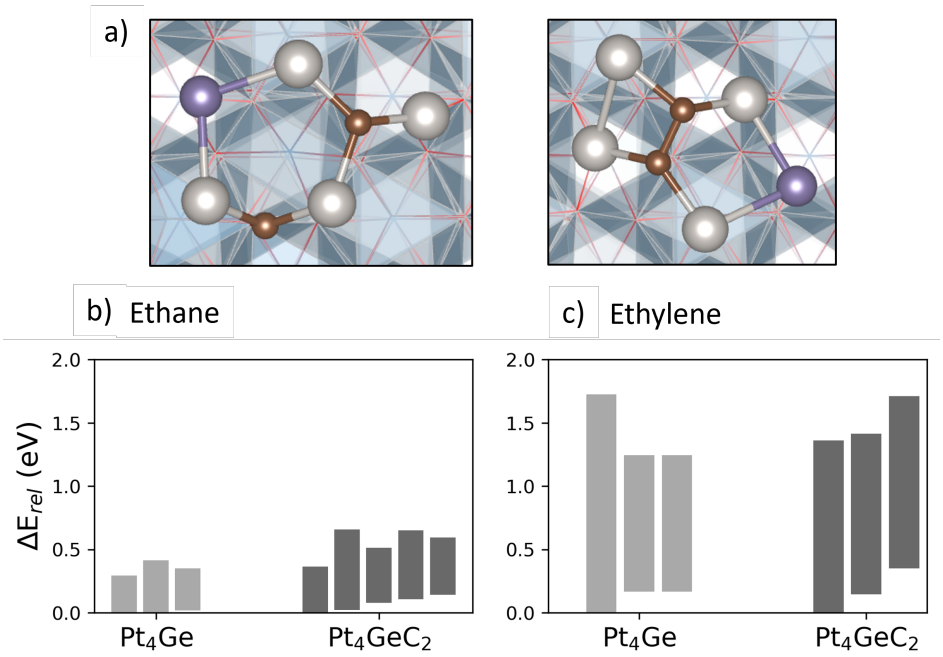

Figure 4: (a) Low-energy isomers of Pt_4GeC_2. Pt atoms are shown in grey, Ge in purple, and C in brown. Blue polyhedra represent the Al_2O_3 support. (b,c) Ethane and ethylene (respectively) C-H activation barriers for Pt_4Ge and Pt_4GeC_2 with individual isomer resolution. The bottom of each bar corresponds to the energy of the reactant isomer, relative to the lowest energy isomer for that composition, and the top of each bar corresponds to the transition state energy.

we compared the barrier heights of C-C cracking to C-H activation starting from the same isomer. These are summarized in Table S1, with relevant barriers shown in Figure S10. For Pt_4 and Pt_4C_2, C-C cracking is only faster than dehydrogenation for for bound acetylene, in agreement with literature.[16,18] For Pt_4Ge and Pt_4GeC_2, on the other hand, we see that the C-C cracking barrier is always higher than the corresponding C-H activation barrier. The addition of Ge therefore eliminates C-C cracking as a possible side-reaction. Doping with Ge and Sn suppresses these side-reactions for bulk and larger NP systems.[39–41] Ge therefore reduces the tendency to coke not only by raising barriers for deeper dehydrogenation, but also by preventing coke-forming side-reactions. This leads to a difference in the kinetic accessibility of the Pt_4C_2 and Pt_4GeC_2 ensembles. Since there are more feasible C-C cracking pathways for Pt_4, the isomer with the split C_2 unit is kinetically accessible, and plays a role in the catalytic behavior of Pt_4C_2. The Pt_4GeC_2 isomer with the split C_2 unit is however not

accessible due to higher C-C cracking barriers, despite the fact that it is the putative global minimum. Thus, relative populations of isomer in the ensemble may be determined by relative rates of dehydrogenation and C-C cracking, rather than by their relative energies. Given the large activity differences between isomers, detailed knowledge of all possible reactions would be necessary for quantitative predictions of non-equilibrium ensemble behaviors. This is in agreement with work by Peters, which emphasizes the importance of isomer interconversion flux and reaction production leading to deviations of populations from their equilibrium concentrations.[42] Thus reactivity may not be identifiable from equilibrium populations alone.

Experimental Support

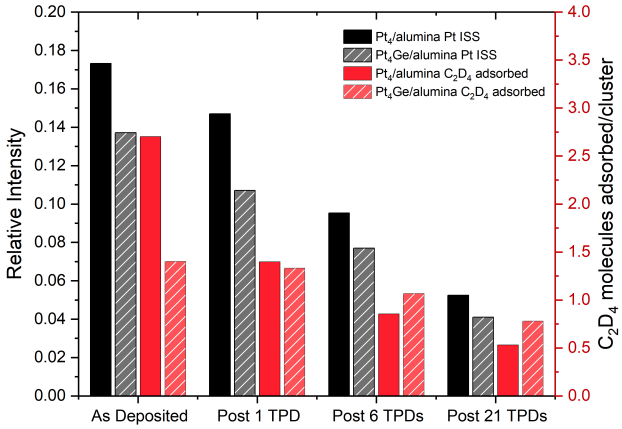

Figure 5: Pt relative intensities from He^+ ion scattering spectroscopy of Pt_4/alumina (black) and Pt_4Ge/alumina (hatched grey). The secondary axis highlights the number of C_2D_4 molecules adsorbed to Pt sites on Pt_4/alumina (red) and Pt_4Ge/alumina (hatched light red) per cluster.

For experimental validation of the electronic origin of the Ge effects on coking and stability, we compare our DFT results to ISS and TPD data for Pt_4 and Pt_4Ge, before and after varying numbers of ethylene TPD cycles.[29] Each cycle involved first saturating the catalysts with C_2D_4 at 180 K, then heating to drive desorption of either intact C_2D_4 or of D_2, the latter indicating carbon deposition. The TPD data is from previous work, and explored in more detail there.[29] In brief- the as-prepared Pt_4 catalyst has a high T desorption peak for

ethylene around 310 K for the first 2 TPD cycles, but which rapidly decreased, indicating rapid loss of strong ethylene binding sites. D_2 desorption also rapidly decreases in successive TPD runs. For Pt_4Ge, in contrast, the high-T ethylene and D_2 desorption features are stable over repeated runs, with much less D_2 desorption compared to Pt_4. This reflects higher stability and selectivity against coking of the Pt_4Ge clusters.

ISS allows us to track changes induced by TPD cycles in in the surface layer of the catalysts, which can be compared to the estimated total number of strong ethylene binding sites per clusters, estimated prior to each TPD cycle (details in SI). For $Pt_{4/}Al_2O_3$, the "as-prepared" Pt ISS intensity reflects a catalyst where essentially all the Pt atoms are in the He^+-accessible surface layer. The Pt intensities were attenuated, relative to those for the as-prepared catalyst, by factors of 15%, 45%, and 70%, respectively, after 1, 6, and 21 TPD runs, reflecting shadowing/blocking of He^+ scattering by bound C atoms. Note, however, that after 6 TPD runs, 6 to 8 C atoms per Pt_4 cluster were estimated to be present,[29] but more than half of the Pt atoms remained He^+-accessible, whereas saturating the Pt clusters with CO molecules resulted in much larger ($\sim$ 80%) attenuation of Pt ISS signals.[26] This supports our results showing restructuring of Pt_4 upon the addition of C_2, which has also been seen experimentally on the surfaces of larger NPs.[43] The number of ethylene molecules adsorbed in strong binding sites decreases more rapidly after each TPD run, by factors of 48%, 68% and 80%, respectively, after 1, 6 and 21 runs. The decline in strong ethylene binding sites is partly offset by an increase in weak binding sites,.[29] Thus, the combination of ISS and TPD suggests that while there is some steric site blocking by carbon deposition, the larger effect on ethylene binding is electronic, decreasing the binding energies such that few strong binding sites remain. Because these strong binding sites are responsible for the dehydrogenation activity, the catalyst deactivates.

For Pt_4Ge the as-prepared ISS intensity was 21% lower than for as-prepared Pt_4, attributed to Ge atoms partially shadowing or blocking He^+ scattering from Pt. The attenuations of the Pt ISS signal, relative to as-prepared Pt_4Ge, were 22%, 44%, and 70% after 1, 6, and

21 TPD runs respectively, similar to Pt_4. In contrast, the loss of strong of ethylene binding sites per Pt_4Ge was much smaller than for Pt_4, at 5%, 24%, and 44%, respectively. Pt_4Ge clusters were estimated to have a total of˜2 C atoms present per cluster after 6 TPDs - just one third of the number deposited per Pt_4. Thus, experiment shows that there is less, but still significant coking on Pt_4Ge, that similar fractions of the initial Pt atoms remain in the surface layer, and that the loss of strong ethylene binding sites is inhibited by Ge. This, too, supports our conclusions that Pt_4Ge restructures upon the addition of C_2, and that the improved stability of Pt_4GeC_2 arises from electronic effects due to the interaction between the Ge, Pt, and C.

Conclusions

We have studied the electronic behavior of four dehydrogenation catalysts, Pt_4, Pt_4C_2, Pt_4Ge, and Pt_4GeC_2, all supported on Al_2O_3, to explore the role that Ge plays in mitigating deactivation via coke formation. Pt_4 is predicted to be a potent ethane dehydrogenation catalyst, but suffers from poor selectivity, driving deep dehydrogenation that leads to carbon deposition and catalyst deactivation. Coke formation induces restructuring of the cluster core, and increases the energy barriers for ethane and ethylene C-H activation, while also decreasing adsorption energies. The partially coked Pt_4C_2 is therefore more selective, but much less active than the uncoked catalyst. This deactivation is attributed to electronic effects, as coke formation does not primarily block sites, but changes the electronic properties of the cluster, with the C_2 unit withdrawing electron density from Pt.

Pt_4Ge is already more selective than Pt_4, due to higher ethylene C-H activation barriers, while retaining the same activity towards ethane. However, it is the interaction between Ge and C_2 that results in "coke-resistance". Pt_4GeC_2 has a similar ethane C-H activation barrier to Pt_4Ge, and even higher ethylene C-H activation barriers. Ge donates electrons to the C_2 unit, preventing the depletion of electron density on Pt, allowing it to retain ac-

tivity despite some coke formation. Additionally, as Ge strengthens the C-C π-bond, the binding of further coke to the C_2 unit is discouraged, as it would require the disruption of the bonding C-C interaction. Thus, Pt_4GeC_2 is an active dehydrogenation catalyst despite carbon deposition, with desirable selectivity arising from the interaction between Ge and C_2. The ab initio results are substantiated by experimental results, which demonstrate that the physical loss of ethylene binding sites during coking is insufficient to explain loss of activity, reflecting that the effect observed for both Pt_4 and Pt_4Ge is electronic rather than steric. The cooperative interaction between Ge and C_2 invites us to see the two species as co-dopants for Pt_4, where Ge as a promoter prevents the poisoning effect of C_2 alone. This conclusion sheds new light on the report in literature that "coke-resistant" Pt-Sn[1,24] or Pt-Ge catalysts[6] remain active despite coke buildup. We believe that the observations reported here may help explain the behavior of a broader class of coke-resistant catalysts, and shoudl be applicable to other compositions and reactions.

Methods

Computational Methods

Calculations on surface-supported clusters were performed using plane-wave DFT in VASP,[44] using the PBE exchange-correlation functional,[45] PAW pseudopotentials,[46] and a plane-wave cut-off of 500 eV. Unit cells were constructed from a 5-layer 3x3 supercell of Al_2O_3 with a 15 Å vacuum gap. Transition states were calculated using the climbing-image nudged elastic band (CI-NEB) method implemented in VTST.[47,48] QTAIM analysis was performed using the Bader code developed by the Henkelman group.[35,49]

Global optimizations were performed with a BLDA approach[50] to generating chemically-reasonable initial structures, both for cluster structure sampling, and adsorbate binding sampling. The in-house codes PGOPT and GOCIA were used to run the optimizations.

Local-basis projections for bonding analysis were performed with LOBSTER,[51] using the

PBEVaspFit basis set and a projection basis of $5p5d6s$ for Pt, $4s4p$ for Ge, $3s3p$ for Al, and $2s2p$ for C and O.[52,53] All projections reported less than 1.2% charge spilling.

DFT calculations on gas-phase models were performed with the Amsterdam Density Functional (ADF) package,[54] version 2019.304, using the PBE functional.[45] Slater-type basis sets of triple-ζ + polarization quality were used on all atoms, with orbitals up to 4d (Pt), 3d (Ge) and 1s (C) included in the frozen core.[55]

Experimental Methods

The relative intensities in He^+ ion scattering spectroscopy (ISS) was summarized from the series of ISS previous results for Pt_4/alumina and Pt_4Ge/alumina.[29] The relative intensities are calculated by taking the average Pt ISS signals of the first 3 data points of the corresponding series of ISS, of which the ISS signals are calculated by integrating the background subtracted Pt integrated intensities normalized to the total integrated ISS signals for the full ion scattering spectrum that remain relatively invariant to compensate for the fluctuation of He + ions scattered. The Pt ISS signals for the as deposited samples are extrapolated, to reveal what the initial Pt ISS signals would be at, from the gradual leveled curve rising from the ISS intensities after some exposure of the samples under He + ions; the extrapolated numbers are close to their corresponding Pt ISS signals post 750 K heat treatment, thus indicating the presence of adventitious adsorbates or H and Cl atoms present on the sample surfaces as well as that the clusters do not sinter much after a single heat treatment on the sample surface.

The C_2D_4 adsorbed molecules per cluster are calculated from the sum of the high temperature C_2D_4 desorption peaks (attributed to C_2D_4 binding to Pt) and half of the D_2 desorbed molecules (as each C_2D_4 produces 2 D_2 molecules) in the temperature programmed desorption from our previous work.[29]

References

Acknowledgement

The authors acknowledge funding from Air Force Office of Scientific Research grant AFOSR FA9550-22-1-0381.

Supporting Information Available

Computed ensembles for Pt_4, Pt_4C_2, Pt_4Ge, and Pt_4GeC_2 both bare and with adsorbed C_2H_6, C_2H_4, and C_2H_2. MO analysis of Pt_4C_2 vs. Pt_4GeC_2. Structures corresponding with C-H activation and C-C cracking NEBs. Comparison between C-H and C-C breaking barriers.

References

(1) Sattler, J. J. H. B.; Beale, A. M.; Weckhuysen, B. M. Operando Raman spectroscopy study on the deactivation of Pt/Al2O3 and Pt–Sn/Al2O3 propane dehydrogenation catalysts. *Physical Chemistry Chemical Physics* **2013**, *15*, 12095.

(2) Zhang, W.; Wang, H.; Jiang, J.; Sui, Z.; Zhu, Y.; Chen, D.; Zhou, X. Size Dependence of Pt Catalysts for Propane Dehydrogenation: from Atomically Dispersed to Nanoparticles. *ACS Catalysis* **2020**, *10*, 12932–12942.

(3) Gorey, T. J.; Zandkarimi, B.; Li, G.; Baxter, E. T.; Alexandrova, A. N.; Anderson, S. L. Preparation of Size- and Composition-Controlled $Pt_n Sn_x/SiO_2$ (n = 4, 7, 24) Bimetallic Model Catalysts with Atomic Layer Deposition. *The Journal of Physical Chemistry C* **2019**, *123*, 16194–16209.

(4) Zandkarimi, B.; Gorey, T. J.; Li, G.; Munarriz, J.; Anderson, S. L.; Alexandrova, A. N.

Alloying with Sn Suppresses Sintering of Size-Selected Subnano Pt Clusters on SiO_2 with and without Adsorbates. *Chemistry of Materials* **2020**, *32*, 8595–8605.

(5) Li, G.; Zandkarimi, B.; Cass, A. C.; Gorey, T. J.; Allen, B. J.; Alexandrova, A. N.; Anderson, S. L. Sn-modification of Pt_7 /alumina model catalysts: Suppression of carbon deposition and enhanced thermal stability. *The Journal of Chemical Physics* **2020**, *152*, 024702.

(6) Huang, Z.; Fryer, J. R.; Park, C.; Stirling, D.; Webb, G. Transmission Electron Microscopy, Energy Dispersive X-Ray Spectroscopy, and Chemisorption Studies of Pt–Ge/γ-Al2O3Reforming Catalysts. *Journal of Catalysis* **1998**, *175*, 226–235.

(7) Jimenez-Izal, E.; Liu, J.-Y.; Alexandrova, A. N. Germanium as key dopant to boost the catalytic performance of small platinum clusters for alkane dehydrogenation. *Journal of Catalysis* **2019**, *374*, 93–100.

(8) Jimenez-Izal, E.; Zhai, H.; Liu, J.-Y.; Alexandrova, A. N. Nanoalloying MgO-Deposited Pt Clusters with Si To Control the Selectivity of Alkane Dehydrogenation. *ACS Catalysis* **2018**, *8*, 8346–8356.

(9) Sattler, J. J. H. B.; Gonzalez-Jimenez, I. D.; Luo, L.; Stears, B. A.; Malek, A.; Barton, D. G.; Kilos, B. A.; Kaminsky, M. P.; Verhoeven, T. W. G. M.; Koers, E. J.; Baldus, M.; Weckhuysen, B. M. Platinum-Promoted Ga/Al_2O_3 as Highly Active, Selective, and Stable Catalyst for the Dehydrogenation of Propane. *Angewandte Chemie International Edition* **2014**, *53*, 9251–9256.

(10) Payard, P.-A.; Rochlitz, L.; Searles, K.; Foppa, L.; Leuthold, B.; Safonova, O. V.; Comas-Vives, A.; Copéret, C. Dynamics and Site Isolation: Keys to High Propane Dehydrogenation Performance of Silica-Supported PtGa Nanoparticles. *JACS Au* **2021**, *1*, 1445–1458.

(11) Raman, N.; Wolf, M.; Heller, M.; Heene-Würl, N.; Taccardi, N.; Haumann, M.; Felfer, P.; Wasserscheid, P. GaPt Supported Catalytically Active Liquid Metal Solution Catalysis for Propane Dehydrogenation–Support Influence and Coking Studies. *ACS Catalysis* **2021**, *11*, 13423–13433.

(12) Cybulskis, V. J.; Bukowski, B. C.; Tseng, H.-T.; Gallagher, J. R.; Wu, Z.; Wegener, E.; Kropf, A. J.; Ravel, B.; Ribeiro, F. H.; Greeley, J.; Miller, J. T. Zinc Promotion of Platinum for Catalytic Light Alkane Dehydrogenation: Insights into Geometric and Electronic Effects. *ACS Catalysis* **2017**, *7*, 4173–4181.

(13) Dadras, J.; Jimenez-Izal, E.; Alexandrova, A. N. Alloying Pt Sub-nano-clusters with Boron: Sintering Preventative and Coke Antagonist? *ACS Catalysis* **2015**, *5*, 5719–5727.

(14) Ha, M.-A.; Baxter, E. T.; Cass, A. C.; Anderson, S. L.; Alexandrova, A. N. Boron Switch for Selectivity of Catalytic Dehydrogenation on Size-Selected Pt Clusters on Al2O3. *J. Am. Chem. Soc.* **2017**, 8.

(15) Aly, M.; Fornero, E. L.; Leon-Garzon, A. R.; Galvita, V. V.; Saeys, M. Effect of Boron Promotion on Coke Formation during Propane Dehydrogenation over Pt/γ-Al2O3 Catalysts. *ACS Catalysis* **2020**, *10*, 5208–5216.

(16) Lian, Z.; Ali, S.; Liu, T.; Si, C.; Li, B.; Su, D. S. Revealing the Janus Character of the Coke Precursor in the Propane Direct Dehydrogenation on Pt Catalysts from a kMC Simulation. *ACS Catalysis* **2018**, *8*, 4694–4704.

(17) Lian, Z.; Si, C.; Jan, F.; Zhi, S.; Li, B. Coke Deposition on Pt-Based Catalysts in Propane Direct Dehydrogenation: Kinetics, Suppression, and Elimination. *ACS Catalysis* **2021**, *11*, 9279–9292.

(18) Nykänen, L.; Honkala, K. Selectivity in Propene Dehydrogenation on Pt and Pt $_3$ Sn Surfaces from First Principles. *ACS Catalysis* **2013**, *3*, 3026–3030.

(19) Yang, M.-L.; Zhu, Y.-A.; Zhou, X.-G.; Sui, Z.-J.; Chen, D. First-Principles Calculations of Propane Dehydrogenation over PtSn Catalysts. *ACS Catalysis* **2012**, *2*, 1247–1258.

(20) Mariscal, R.; Fierro, J. L.; Yori, J. C.; Parera, J. M.; Grau, J. M. Evolution of the properties of PtGe/Al2O3 reforming catalysts with Ge content. *Applied Catalysis A: General* **2007**, *327*, 123–131.

(21) Ballarini, A. D.; de Miguel, S.; Castro, A.; Scelza, O. n-decane dehydrogenation on bimetallic PtSn and PtGe catalysts prepared by dip-coating. *Catalysis in Industry* **2013**, *5*, 283–296.

(22) Hook, A.; Celik, F. E. Predicting Selectivity for Ethane Dehydrogenation and Coke Formation Pathways over Model Pt–M Surface Alloys with ab Initio and Scaling Methods. *The Journal of Physical Chemistry C* **2017**, *121*, 17882–17892.

(23) Borgna, A.; Garetto, T.; Apesteguia, C. Simultaneous deactivation by coke and sulfur of bimetallic Pt–Re(Ge, Sn)/Al2O3 catalysts for n-hexane reforming. *Applied Catalysis A: General* **2000**, *197*, 11–21.

(24) Kumar, M. S.; Chen, D.; Holmen, A.; Walmsley, J. C. Dehydrogenation of propane over Pt-SBA-15 and Pt-Sn-SBA-15: Effect of Sn on the dispersion of Pt and catalytic behavior. *Catalysis Today* **2009**, *142*, 17–23.

(25) Zandkarimi, B.; Alexandrova, A. N. Dynamics of Subnanometer Pt Clusters Can Break the Scaling Relationships in Catalysis. *Journal of Physical Chemistry Letters* **2019**, *10*, 460–467.

(26) Baxter, E. T.; Ha, M.-A.; Cass, A. C.; Alexandrova, A. N.; Anderson, S. L. Ethylene Dehydrogenation on Pt $_{4,7,8}$ Clusters on Al $_2$ O $_3$: Strong Cluster Size Dependence Linked to Preferred Catalyst Morphologies. *ACS Catalysis* **2017**, *7*, 3322–3335.

(27) Jo, Y.; Kim, T. W.; Oh, J.; Kim, D.; Suh, Y.-W. Mesoporous sulfur-decorated Pt–Al2O3 for dehydrogenation of perhydro benzyltoluenes: Activity-favorable adsorption of reaction species onto electron-deficient Pt atoms. *Journal of Catalysis* **2022**, *413*, 127–137.

(28) Zhai, H.; Alexandrova, A. N. Local Fluxionality of Surface-Deposited Cluster Catalysts: The Case of Pt7 on Al2O3. *The Journal of Physical Chemistry Letters* **2018**, *9*, 1696–1702.

(29) Li, G.; Poths, P.; Masubuchi, T.; Morgan, H.; Alexandrova, A.; Anderson, S. L. Got Coke? Self-Limiting Poisoning Makes an Ultra Stable and Selective Sub-nano Cluster Catalyst. **2022**,

(30) Liu, G. X.; Poths, P.; Zhang, X. X.; Zhu, Z. G.; Marshall, M.; Blankenhorn, M.; Alexandrova, A. N.; Bowen, K. H. CO_2 Hydrogenation to Formate and Formic Acid by Bimetallic Palladium-Copper Hydride Clusters. *Journal of the American Chemical Society* **2020**, *142*, 7930–7936.

(31) Halder, A.; Ha, M. A.; Zhai, H. C.; Yang, B.; Pellin, M. J.; Seifert, S.; Alexandrova, A. N.; Vajda, S. Oxidative Dehydrogenation of Cyclohexane by Cu vs Pd Clusters: Selectivity Control by Specific Cluster Dynamics. *Chemcatchem* **2020**, *12*, 1307–1315.

(32) Zhang, Z.; Zandkarimi, B.; Alexandrova, A. N. Ensembles of Metastable States Govern Heterogeneous Catalysis on Dynamic Interfaces. *Accounts of Chemical Research* **2020**, *53*, 447–458, Publisher: American Chemical Society.

(33) Lavroff, R. H.; Morgan, H. W. T.; Zhang, Z.; Poths, P.; Alexandrova, A. Ensemble representation of catalytic interfaces: soloists, orchestras, and everything in-between. *Chemical Science* **2022**,

(34) Carey, F. A.; Sundberg, R. J. *Advanced Organic Chemistry*; Springer US, 1990.

(35) Bader, R. F. W. A quantum theory of molecular structure and its applications. *Chemical Reviews* **1991**, *91*, 893–928.

(36) Wikipedia contributors, Electronegativity — Wikipedia, The Free Encyclopedia. 2022; `https://en.wikipedia.org/w/index.php?title=Electronegativity&oldid=1096663220`.

(37) Muller, P. C.; Ertural, C.; Hempelmann, J.; Dronskowski, R. Crystal Orbital Bond Index: Covalent Bond Orders in Solids. *Journal of Physical Chemistry C* **2021**, *125*, 7959–7970.

(38) Sattler, J. J. H. B.; Ruiz-Martinez, J.; Santillan-Jimenez, E.; Weckhuysen, B. M. Catalytic Dehydrogenation of Light Alkanes on Metals and Metal Oxides. *Chemical Reviews* **2014**, *114*, 10613–10653.

(39) Hook, A.; Massa, J. D.; Celik, F. E. Effect of Tin Coverage on Selectivity for Ethane Dehydrogenation over Platinum–Tin Alloys. *The Journal of Physical Chemistry C* **2016**, *120*, 27307–27318.

(40) Wang, Z.; Chen, Y.; Mao, S.; Wu, K.; Zhang, K.; Li, Q.; Wang, Y. Chemical Insight into the Structure and Formation of Coke on PtSn Alloy during Propane Dehydrogenation. *Advanced Sustainable Systems* **2020**, *4*, 2000092.

(41) Furukawa, S.; Tamura, A.; Ozawa, K.; Komatsu, T. Catalytic properties of Pt-based intermetallic compounds in dehydrogenation of cyclohexane and n-butane. *Applied Catalysis A: General* **2014**, *469*, 300–305.

(42) Peters, B. Simple Model and Spectral Analysis for a Fluxional Catalyst: Intermediate Abundances, Pathway Fluxes, Rates, and Transients. *ACS Catalysis* **2022**, *12*, 8038–8047.

(43) Wu, J.; Helveg, S.; Ullmann, S.; Peng, Z.; Bell, A. T. Growth of encapsulating carbon on supported Pt nanoparticles studied by in situ TEM. *Journal of Catalysis* **2016**, *338*, 295–304.

(44) Kresse, G.; Furthmuller, J. Efficient iterative schemes for ab initio total-energy calculations using a plane-wave basis set. *Physical Review B* **1996**, *54*, 11169–11186.

(45) Perdew, J. P.; Burke, K.; Ernzerhof, M. Generalized gradient approximation made simple. *Physical Review Letters* **1996**, *77*, 3865–3868.

(46) Blochl, P. E. Projector augmented wave method. *Physical Review B* **1994**, *50*, 17953–17979.

(47) Sheppard, D.; Xiao, P. H.; Chemelewski, W.; Johnson, D. D.; Henkelman, G. A generalized solid-state nudged elastic band method. *Journal of Chemical Physics* **2012**, *136*, 8.

(48) Henkelman, G.; Uberuaga, B. P.; Jonsson, H. A climbing image nudged elastic band method for finding saddle points and minimum energy paths. *Journal of Chemical Physics* **2000**, *113*, 9901–9904.

(49) Tang, W.; Sanville, E.; Henkelman, G. A grid-based Bader analysis algorithm without lattice bias. *Journal of Physics-Condensed Matter* **2009**, *21*.

(50) Zhai, H.; Alexandrova, A. N. Ensemble-Average Representation of Pt Clusters in Conditions of Catalysis Accessed through GPU Accelerated Deep Neural Network Fitting Global Optimization. *Journal of Chemical Theory and Computation* **2016**, *12*, 6213–6226.

(51) Maintz, S.; Deringer, V. L.; Tchougréeff, A. L.; Dronskowski, R. LOBSTER: A tool to extract chemical bonding from plane-wave based DFT. *Journal of Computational Chemistry* **2016**, *37*, 1030–1035.

(52) Dronskowski, R.; Blochl, P. E. Crystal orbital Hamiltonian populations (COHP) - Energy-resolved visualization of chemical bonding in solids based on density-functional calculations. *Journal of Physical Chemistry* **1993**, *97*, 8617–8624.

(53) Deringer, V. L.; Tchougreeff, A. L.; Dronskowski, R. Crystal Orbital Hamilton Population (COHP) Analysis As Projected from Plane-Wave Basis Sets. *Journal of Physical Chemistry A* **2011**, *115*, 5461–5466.

(54) te Velde, G.; Bickelhaupt, F. M.; Baerends, E. J.; Guerra, C. F.; Van Gisbergen, S. J. A.; Snijders, J. G.; Ziegler, T. Chemistry with ADF. *Journal of Computational Chemistry* **2001**, *22*, 931–967.

(55) Van Lenthe, E.; Baerends, E. J. Optimized Slater-type basis sets for the elements 1-118. *Journal of Computational Chemistry* **2003**, *24*, 1142–1156.

TOC Graphic

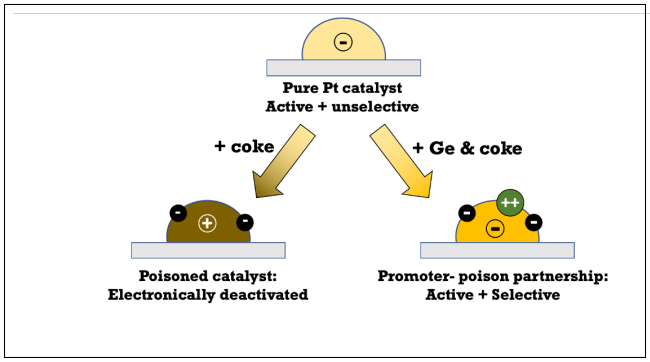
Pure Pt catalyst
Active + unselective
+ coke
+ Ge & coke
Poisoned catalyst:
Electronically deactivated
Promoter- poison partnership:
Active + Selective